Chem

CellPress

Article

Single-molecule mechanics of synthetic aromatic amide helices: Ultrafast and robust non-dissipative winding

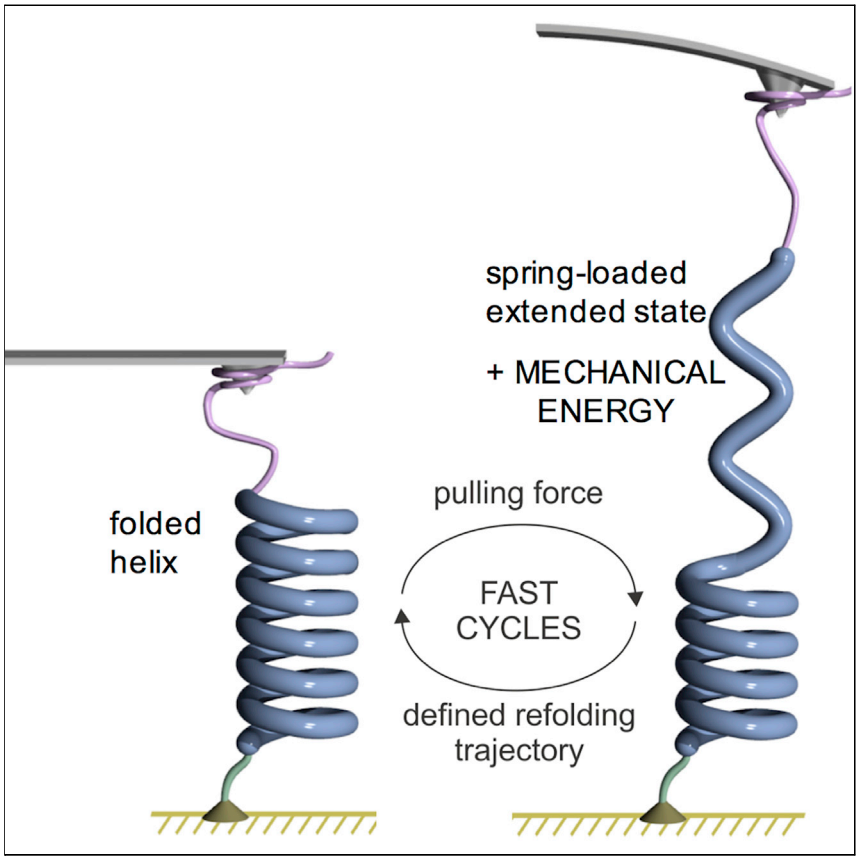

Helices are crucial structural components that contribute to protein elasticity and motor functions. Numerous artificial helices based on backbones other than peptides and much smaller than proteins have been synthesized, yet, their mechanical performance is essentially unknown. Here, we report that the elastic response of helical aromatic oligoamides as small as 1 nm is among the fastest and the most robust ever described. Their winding is reversible on a very short time scale even under high mechanical loads, in contrast with typical biopolymers.

Floriane Devaux, Xuesong Li, Damien Sluysmans, ..., Francesco Zerbetto, Ivan Huc, Anne-Sophie Duwez

ivan.huc@cup.lmu.de (I.H.)
asduwez@uliege.be (A.-S.D.)

Highlights

Single-molecule force spectroscopy probes the mechanics of 1-nm-size synthetic helices

Outstanding elasticity and rewinding capabilities of aromatic amide helices

Ultrafast nondissipative winding along precise trajectories

Reducing molecular size does not compromise mechanical properties

Devaux et al., Chem 7, 1333–1346
May 13, 2021
https://doi.org/10.1016/j.chempr.2021.02.030

Chem

CellPress

Article

Single-molecule mechanics of synthetic aromatic amide helices: Ultrafast and robust non-dissipative winding

Floriane Devaux,[1,2] Xuesong Li,[1,2] Damien Sluysmans,[1] Victor Maurizot,[2] Evangelos Bakalis,[3] Francesco Zerbetto,[3] Ivan Huc,[2,4,5,*] and Anne-Sophie Duwez[1,6,*]

SUMMARY

Because of proteins' many degrees of conformational freedom, programming protein folding dynamics, overall elasticity, and motor functions remains an elusive objective. Instead, smaller and simpler objects, such as synthetic foldamers, may be amenable to design. However, little is known about their mechanical performance. Here, we show that reducing molecular size may not compromise mechanical properties. We report that helical aromatic oligoamides as small as 1 nm possess outstanding elasticity and outperform most natural helices. Using single-molecule force spectroscopy, we characterize their folding trajectories and intermediate states. We show that they cooperatively and reversibly unwind at high forces. They extend up to 3.8 times their original length and rewind against considerable forces on a timescale of 10 μs. Pulling and relaxing cycles follow the same trace up to a very high loading rate, indicating that the mechanical energy accumulated during the stretching does not dissipate and is immediately reusable.

INTRODUCTION

Folding is the process by which the three-dimensional shapes and properties of proteins are generated from linear peptide chains. Folding is reversible and allows for some important dynamics to take place: molecular shape changes determine mechanical and motor functions in living systems. For example, reversible conformational changes in titin and elastin have been associated with tissue elasticity.[1,2] Conversely, the stiffness of collagen is responsible for tissue resistance.[3] While there has been a considerable progress in the design of new protein folds,[4] programming protein folding dynamics has remained an elusive objective because of the co-existence of multiple folding trajectories and of local energy minima, which slow down the process and compromise refolding on a short time scale. Smaller folded objects than proteins may provide entries into simpler folding dynamics and thus amenability to design. For example, the peptidic α-helix and nucleic acid helices have both been investigated in detail and show different behaviors intimately associated with their distinct chemical nature.[5–7] For these studies, AFM-based single-molecule force spectroscopy has emerged as a powerful method to probe molecular-level processes and mechanical forces with sub-nanometer resolution in (bio)-macromolecules.[8–14] In principle, all kinds of conformational transitions may give access to energy-dependent structural changes[15] and to some elasticity, e.g., gauche-anti conformational transitions in poly(ethylene oxide) (PEO)[16] or bond bending, rotation, and boat-chair conformations in polysaccharides.[17,18] But systems that would both adopt stable folded conformations that sustain high mechanical forces and

The bigger picture

Chemistry excels in designing and controlling molecular structures. Beyond structure, programming molecular dynamics is one of the next grand challenges. The conformation dynamics of natural elastomeric proteins, for example, are responsible for their ability to behave either as pure elastic spring-like molecules that can be reversibly stretched or as shock absorbers that dissipate energy. Here, we report the outstanding mechanical performances of synthetic helical molecules much smaller than proteins. The molecules were designed for interfacing with AFM force spectroscopy to study them one at a time, a true performance for such tiny objects. We show that the elastic response of helices as small as 1 nm is among the fastest and the most robust ever described. This unprecedented elastic behavior suggests that various applications may arise from their use as building blocks in molecular machines or in new classes of artificial elastomeric materials with tailored mechanical properties.

undergo very fast reversible transitions between unfolded and folded states following well-defined pathways are yet to be reported. For this purpose, molecules having fewer degrees of freedom and steeper conformational energy landscapes than biopolymers would stand as valid candidates. In this respect, it is striking that the molecular mechanical properties of the numerous oligomeric and polymeric foldamers developed by chemists over the years, have not been investigated.[19–22] A reason for this is that implementing single-molecule force spectroscopy on synthetic molecules much smaller than biopolymers remains very challenging: interfacing a small object with the force spectroscopy device and measuring transitions of minute amplitudes are both difficult. A few unfolding experiments have been carried out on relatively small (bio)molecules but they did not probe molecular elasticity and mechanical properties.[23–25] To this date, very few single-molecule mechanics experiments have been successfully conducted on small molecules.[26–29]

Here, we report on the high-performance single-molecule mechanics of helical aromatic oligoamides[30–32] as a representative of the broad family of foldamer backbones that possess aryl rings in their main chain. This emerging class of folded molecules are characterized by remarkably stable and predictable conformations. Many of them wind into helices in which aromatic rings stack face to face.[33–36] We now show that their folding trajectories are simple and may be amenable to design. Using AFM-based single-molecule force spectroscopy, we pulled on helical quinoline-based oligoamides of different lengths to investigate their mechanical properties. We found that their winding is extremely robust and fully reversible on a very short time scale, in contrast with typical biopolymer behavior (Figure 1A). The molecular helices behaved as springs that are energy loaded in their extended states. A detailed analysis, based, among others, on elements of stochastic calculus, allowed us to decipher precise winding/unwinding trajectories at the sub-molecular level and cooperative effects responsible for the observed elasticity. The analysis shows that at short times both winding and unwinding processes are driven by the same stochastic mechanisms. It also shows that at longer times a differentiation of mechanisms occurs. Such well-defined conformational trajectories open up new capabilities to orchestrate motion at the molecular scale.

RESULTS AND DISCUSSION

Molecular helix design

Oligoamides of 8-amino-2-quinolinecarboxylic acid **Q** (Figure 1C) were selected because their structures are well defined, and because their rigidity hinted at simple conformational dynamics. Q_n oligomers adopt defectless helical conformations comprised of 2.5 quinoline units per turn that show high stability in a wide range of solvents.[33,37] Electrostatic repulsions, bifurcated hydrogen bonds, aryl-amide conjugation, and interactions between stacked aromatic rings synergistically concur to this high stability. For example, a simple octamer spanning about three helix turns shows no sign of denaturation at 120°C in DMSO.[33] Furthermore, helix stability rapidly increases with oligomer length.[38,39] The small number of units per turn, i.e., the high helix curvature, endows relatively short sequences with an aspect ratio larger than that of less curved helices,[34,35] and reduces the number of rotatable bonds per turn. Furthermore, stepwise segment-doubling synthesis of these oligomers gives access to long sequences with a perfectly uniform constitution.[40] Variants of these helices bearing specific terminal functions and side-chain or main-chain features display potentially useful properties in contexts as diverse as DNA mimicry and enzyme inhibition,[41] endomolecular recognition,[42] and fast charge transport.[43,44] For this study, four oligomers comprised of 5, 9, 17, and 33 units were prepared (Figures 1C, S1, and S17–S32 and Supplemental experimental procedures). Monomers

[1]UR Molecular Systems, Department of Chemistry, University of Liège, 4000 Liège, Belgium

[2]CBMN Laboratory, University Bordeaux, CNRS, IPB, Institut Européen de Chimie et Biologie, 33600 Pessac, France

[3]Dipartimento di Chimica "G. Ciamician", Università di Bologna, 40126 Bologna, Italy

[4]Department of Pharmacy, Ludwig-Maximilians-Universität, 81377 München, Germany

[5]Cluster of Excellence e-Conversion, 85748 Garching, Germany

[6]Lead contact

*Correspondence: ivan.huc@cup.lmu.de (I.H.), asduwez@uliege.be (A.-S.D.)

https://doi.org/10.1016/j.chempr.2021.02.030

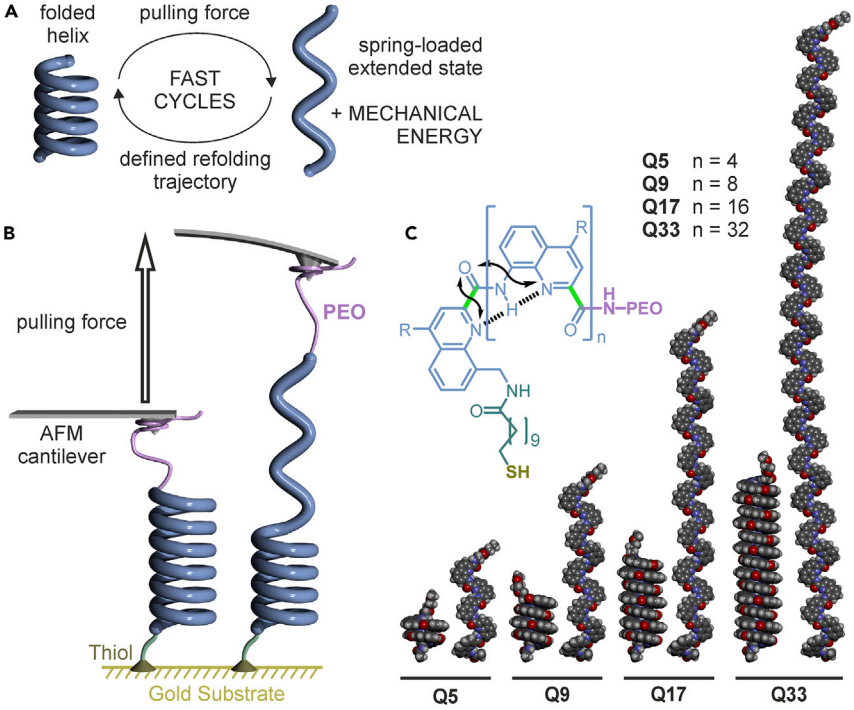

Figure 1. Principle of AFM-based single-molecule force spectroscopy experiments on helices of various lengths

(A) Schematic representation of fast and well-defined folding dynamics. The fastest cycles, at the upper limit of instrumentation, are still slow as compared with the molecular response.

(B) Bending of the AFM cantilever resulting from pulling a single helical molecule attached to a gold substrate.

(C) Formula of oligoamides Q5-Q33 functionalized with a PEO chain at one extremity and a thiol group at the other. R denotes solubilizing isobutoxy chains. Hydrogen bonds and electrostatic repulsions that drive helical folding are indicated with dashes and double-headed arrows, respectively. Cα–CO bonds that are easiest to rotate are shown in green. Molecular models of the helical conformations and the zig-zag tape extended conformations of Q5-Q33 are shown at the bottom. Isobutoxy chains are omitted for clarity.

are δ- or ε-amino acids and equivalent in size to a dipeptide. Thus, even the longest sequence, Q33, is much smaller than proteins investigated so far by single-molecule force spectroscopy. All sequences bear a thiol group at their N terminus to ensure stable attachment to gold substrates, and polyethylene oxide (PEO) at the C terminus to be linked to the AFM tip for pulling. The molecules were grafted onto gold/silicon substrates at low grafting density to ensure large interspaces between them (Figure 1B, See Supplemental information for details). The AFM tip was brought into contact with the oligoamide-PEO substrate in *N*,*N*-dimethylformamide (DMF) to allow the linker to adsorb onto the tip. The caught molecule was then stretched in a controlled manner by moving the tip away from the substrate at a fixed pulling rate, and the force-extension profiles were measured. PEO behaves as a purely random coil in DMF and does not show specific features in the force curves.[26,27] Any deviation from this behavior can thus be safely attributed to the oligoamide helix.

Unwinding behavior reveals cooperativity

Force-extension profiles revealed a consistent behavior for all four foldamers. A typical profile can be divided into different steps (Figure 2A). We attributed the initial part of the force-extension curve (up to about 100 pN) to the unraveling of

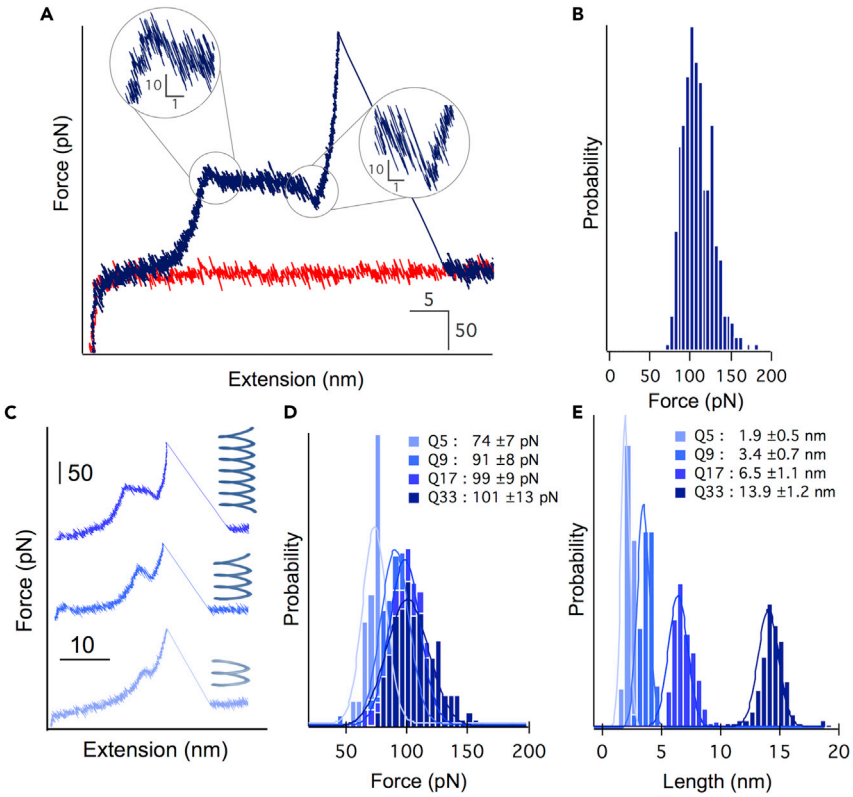

Figure 2. Mechanical unwinding of helices in DMF

(A) Force-distance curve of Q33. Pulling curve (blue) and approaching curve (red) are shown, as well as zooms on the fluctuations at the beginning and at the end of the plateau. Pulling rate: 160 nm·s^{-1}.

(B) Histogram of the force of the unwinding plateau of Q33. The most probable value is 101 ± 13 pN (SD). n = 373.

(C) Force-distance curves of Q17 (dark blue), Q9 (middle blue), and Q5 (light blue). Pulling rate: 160 nm·s^{-1}.

(D) Histograms of the force of the unwinding signal with the most probable value, obtained by Gaussian fit to the data.

(E) Histograms of the length of the unwinding plateau with the most probable value, obtained by Gaussian fit to the data. n = 141 for Q5, n = 349 for Q9, n = 477 for Q17 and n = 373 for Q33. See also Figures S2 and S5–S7.

the PEO random coil and the subsequent plateau to the unwinding of the helical structure. The occurrence of a plateau is characteristic of the breaking of intramolecular interactions in series and is thus usually associated to a non-cooperative unfolding. However, here, the plateau is slightly tilted toward lower forces when the distance increases (Figures 2A, 2C, and S2). It means that it gets easier and easier to open the helix in the course of the unwinding, a signature of a cooperative effect. Once an interaction is broken, the subsequent one is easier to break. At the end of the plateau, the force decreases below plateau level and fluctuates (see next section below). The length of the plateau is in a very good agreement with the theoretical difference in length between the wound and fully extended structures (Figures 1C and S3; Table S1. See Supplemental information for the details of calculation): the extended conformation is 3.8 times longer than the helical state. At the end of the plateau, the helix is completely unwound, and the force rises again as the PEO stretching continues. The force of unwinding, 101 pN for Q33 (Figure 2B), is much higher than for natural helices. For example, double-helical coiled-coil protein

structures, triple-helical spectrin repeats, parallel-stacked α-helical ankyrin repeats, and myomesin α-helical linkers in muscles exhibit unwinding forces of about 20 pN at comparable loading rates.[45–49] The unwinding of long *B*-DNA takes place at 65 pN[50,51] and helical structures in polysaccharides unwind between 20 and 60 pN.[52,53] Force-extension profiles of the foldamers obtained in other solvents (toluene, ethanol, tetrachloroethane, dimethylsulfoxide, acetonitrile, and water) show similar features, evidencing the robustness of the winding in a wide range of media (Figure S4).

The force profiles for the shorter helices are shown in Figures 2C–2E. For Q17, we observed the same characteristic force curves with the length of the plateau being proportional to the length of the molecule (Figures 2E and S2). Q9 displayed a small plateau followed by predominant large fluctuations (Figure S5). Q5 showed only fluctuations or a single rupture peak between the two states (Figure S6), which confirms the cooperativity. The histograms of the length of unwinding signal for each helix show Gaussian-like monomodal distributions centered on a value proportional to the number of units in the helix (Figure 2E). This observation implies that all the helices adopt a unique wound structure in DMF, in agreement with earlier solution and solid-state studies.[32,33] Indeed, narrow monomodal distributions exclude the possibility of populated partially unfolded or differently folded conformations in solution. The unwinding force ranges from 74 to 101 pN from the smallest to the longest helix (Figure 2D). The average unwinding force increases with the number of quinoline units until it reaches a maximum value between 9 and 17 units and plateaus between 17 and 33 units. This is probably an additional signature of cooperativity in winding. Such effects had never been identified in earlier experimental ensemble studies because completely unwound conformations were never reached, only partly unwound transition states were identified. For instance, helix handedness inversion was shown to proceed through a nucleation-propagation mechanism involving the unwinding of only two units.[38,39]

Rewinding states occur at high speed under high forces

Before the plateau starts, we often observed fluctuations (Figures 2A and S7). These fluctuations can be explained by the reforming of an interaction a short time after being broken, and thus occur between wound and partially unwound states. It means that during pulling, the oligoamide pulls on the AFM cantilever in the opposite direction and rewinds against the mechanical load. The average force in the hopping region was about 10 pN higher than the plateau force. This difference in force can be associated to a barrier to overcome in order to trigger the unwinding of the helix. Such a barrier has been described by molecular dynamics simulations and was shown to correspond to the spring-like deformation of the helix.[54] Then, the force decreases, and the plateau starts. At the end of the plateau, the force largely decreases (about 30 pN), and we again detect significant hopping states. In this phase, unwinding requires a lower force and a segment of the foldamer dynamically fluctuates between a partially unwound and the fully unwound state. This is a clear signature of the cooperativity of mechanical unwinding: when the interactions are progressively broken, the subsequent opening is facilitated. The interactions weaken progressively as neighboring interactions disappear along the extension. Weaker forces are thus sufficient to unfold the last part of the sequences, and the drop in force is significant when the length reaches less than two turns. At the upper limit of sampling rate (4,200 $nm \cdot s^{-1}$), we measured a fluctuation rate between wound and unwound states of about 7,500 s^{-1} at forces of 100 pN (Figure 3A). From these fluctuations, we could estimate a minimum rewinding rate of about 25,000 s^{-1} under a force of 100 pN (see Supplemental information for details of the analysis). This

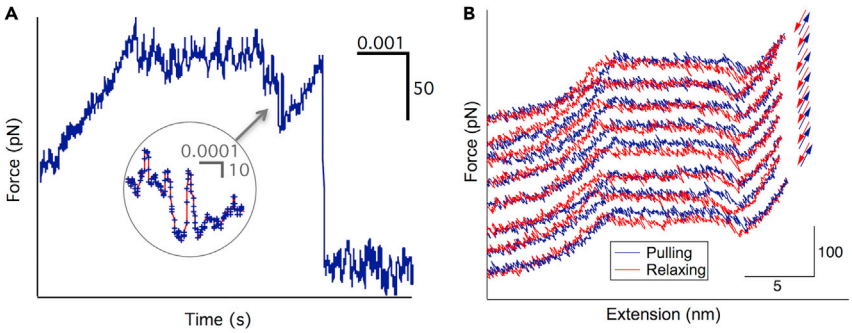

Figure 3. Fast helix rewinding

(A) Force-time pulling curve of Q33 at the fastest pulling rate of 4,200 nm·s^{-1}. Fluctuations are still observable. The step time is 3 μs.

(B) Successive pulling-relaxing cycles showing the immediate rewinding of the helix under mechanical load. Pulling (in blue)-relaxing (in red) curves of Q33 in DMF at 166 nm·s^{-1}. The cycles are offset for clarity. The arrows on the right show the displacement of the cantilever regarding the substrate.

estimation is a lower limit. We were indeed limited by the response time of the cantilever and the sampling rate (Figure S14). It means that the rewinding may be even faster than our estimation. The fastest folding kinetics for single α-helices that has been reported so far by direct time-resolved experimental measurements of fluctuations was 30,000 s^{-1} for villin, an actin-binding protein. This rate is thus comparable to the one obtained here (25,000 s^{-1}), but it was measured at a much lower force of 10 pN.[55] As the folding rate is known to drastically decrease when the applied force increases,[46] we can conclude that the aromatic amide helices are faster to rewind than those natural single α-helices. It is worth mentioning that here we compare the aromatic amide helices, which are single isolated helices, with natural single α-helices only. Other protein structures described in the literature, such as β-sheets, trimeric α-helices in spectrin, and a series of α-helices in bacteriorhodopsin proteins, have also been shown to refold rapidly but against lower forces.[49,56,57] For these proteins, the refolding rate was not measured directly from fluctuations, but estimated from theoretical models to fit the energy landscape. Moreover, the contribution of the inter-helix interactions in these structures is difficult to assess. For these reasons, a direct comparison with the refolding rate measured here is too hazardous.

The distance over which the fluctuations take place at the end of the plateau, about 2 nm, is similar in Q33, Q17, and Q9 (Figure S8). This explains the apparent larger tilt of the plateau for Q9, the contribution of the force drop being thus relatively greater for shorter oligomers (Figures 2C and S5). This distance of 2 nm matches with the extension of 6 quinoline units. We can thus conclude that to observe a plateau characteristic of the sequential opening of the intramolecular interactions, a minimum of 7 units is required. In wound structures shorter than 7 units, the cooperativity results in a rapid change of the force required for unwinding versus helix length, and the intramolecular interactions no longer break in series but all at once.

Complete rewinding is also fast and reveals high elasticity

When a single molecule is trapped between the tip and the substrate, retraction-approach cycles can be performed repeatedly. The eight successive cycles shown in Figure 3B evidence the full reversibility of the unwinding and the robustness of the system. They demonstrate high structural stability: the unwound molecule rewinds instantaneously as tension is released. The force-extension profile of relaxation follows the same trace as during pulling, up to a loading rate of 5.10^4 pN s^{-1} (upper

limit of the instrumentation). The molecule reversibly extends to 3.8 times its original length. Because the stretching process occurs under equilibrium conditions, the area underneath the plateau reflects the free-energy changes associated with the transition. The equilibrium force-extension curves thus allowed us to determine the gain in free energy associated with the formation of the Q33 helix by integrating the force versus extension under the curve and removing the molecular elasticity contribution (see Supplemental information for the details and Figure S15). We obtained a value of 150 ± 14 kcal mol^{-1} (250 ± 20 k_BT) for the whole helix, which is huge compared with values observed in natural α-helices of similar length (typically 16 k_BT).[43]

Unwinding pathways

To characterize the unwinding molecular energy landscape, we performed a transformation of force spectroscopy data from extension space into contour length space. The new molecular coordinate is independent of varying external parameters, such as thermal fluctuations and instrumental parameters, and directly reflects the folding state of the molecule.[46,58] The representation with respect to this molecular coordinate does not exhibit the variances of the extension but directly characterizes the intermediate states of the folding potential. The force-extension data of the plateau (Figures 4A and S9–S11) were converted in contour length (L_c) space by solving numerically the worm-like chain equation (see Supplemental information for details). On the contour length traces (Figure 4A), we observed steady states (marked off by the dotted vertical lines) before and after the plateau, whereas the L_c value increased incrementally along the plateau. The contour length values can be well fitted by Gaussian distributions (Figures 4A and S9–S11). Since one value of L_c can be associated to one state, the number of Gaussian peaks shows the number of states during winding. On an average, we observed 17 ± 2 states for Q33, 8 ± 1 for Q17, 4 ± 0.5 for Q9, and 2 ± 0.5 for Q5.

These results suggest that successive states differ from each other by the unwinding of 2 quinoline units, likely *via* the coupled rotations of Cα–CO bonds, in a good agreement with force-probe molecular dynamics simulations on similar foldamers,[59] and with the geometrical properties of the $\mathbf{Q_n}$ helices (Figure 5). Four units can also unwind simultaneously, as some vertical transitions between two non-successive states are sometimes observed. These transitions are reversible, which is in agreement with the hopping behavior discussed above. They take place more often for Q9 and Q5, and at the end of the unwinding pattern for the longer helices, supporting our previous conclusion that the cooperativity does not increase beyond a certain helix length. A detailed analysis of the unwinding behavior of Q5 corroborates this interpretation: two types of signatures can be observed in its force-distance curves, either a single rupture peak, or fluctuations (Figure S6). When a single rupture peak is detected, we observe only the two extreme states (fully wound and fully unwound) in the contour length trace, whereas a third intermediate state is visible in the contour length trace when fluctuations are detected in the force-distance curve (Figures S10 and S11).

A more detailed visualization of unwinding pathways can be achieved by means of the cross-superposition of 2D barrier position histograms (Figure 4B). This method has been proposed previously to detect the order of unfolding events in proteins.[58] The energy barriers appear as stripes (Figure 4B and Supplemental information for details about the procedure). The smallest rectangles, formed by matching contour length increments from two experiments (first possible match of the n L_c value and the last possible match of the n+1 L_c value), are determined. If subsequent rectangles are aligned with the diagonal with positive slope, the same unwinding steps occur for

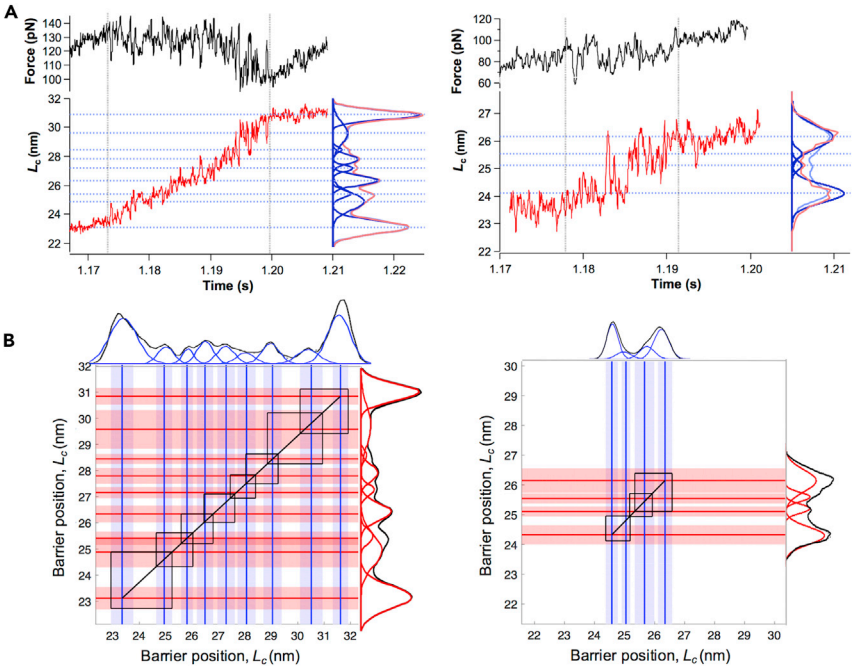

Figure 4. Unwinding molecular energy landscape and cross-superposition of barrier position histograms

(A) Force versus time curve of Q17 (left panel) and Q9 (right panel) unwinding area (black trace) and contour length evolution of the intermediate unwinding states represented as a function of time (red trace). On the right of each panel, the corresponding contour length histogram (light red), the multi-Gaussian peaks fitting the histogram (blue) and the overall fit trace (light blue). The dotted blue lines are the L_c values of the intermediate unwound states (most probable values of the Gaussian fits).

(B) Cross-superposition of two histograms of L_c distributions for Q17 (left panel) and Q9 (right panel). Red and blue lines represent the mean L_c values of the Gaussian fits of the L_c histograms with their 70% confidence interval (light red and light blue stripes). Similar unwinding steps from different experiments are determined by drawing rectangles between intersected L_c value increments. If these intersections occur on the diagonal (black line) it implies that the same unwinding steps occur for both unwinding patterns. Taking into account the confidence interval, the black rectangles comprise every potential pathway along each unwinding step.

both unwinding patterns. According to the cross-superposition of contour length traces of the unwinding patterns of different experiments (Figures 4B, S12, and S13) and previous simulations,[59] we can conclude that the unwinding occurs most of the time by the same pathway, i.e., the rotation of 2 units. However, we can occasionally observe partially different pathways (Figures S12 and S13). Therefore, although unwinding by the rotation of 2 units appears to be the most probable pathway, it may also occur by the rotation of a single Cα–CO bond or by more than two bonds. In all likelihood, this occurs at either end of the helix, and thus defines a limited ensemble of unwinding trajectories. For short helices, the few intermediate states reduce the number of possible pathways (Figure 4B, right panel). It should be specified that the information given by the 2D graphs only shows that the unwinding takes place through sequences of 2 quinoline units but does not give any information on the sequence of unwinding. Each individual unwinding sequences of 2 units has an equal probability to take place at any given time, earlier or later.

Analysis of time series in terms of stochastic processes

The plateaus of the pulling-relaxing forces versus time of Figure 3B were analyzed as stochastic sequences with the anomalous diffusion object motion analysis, ADOMA

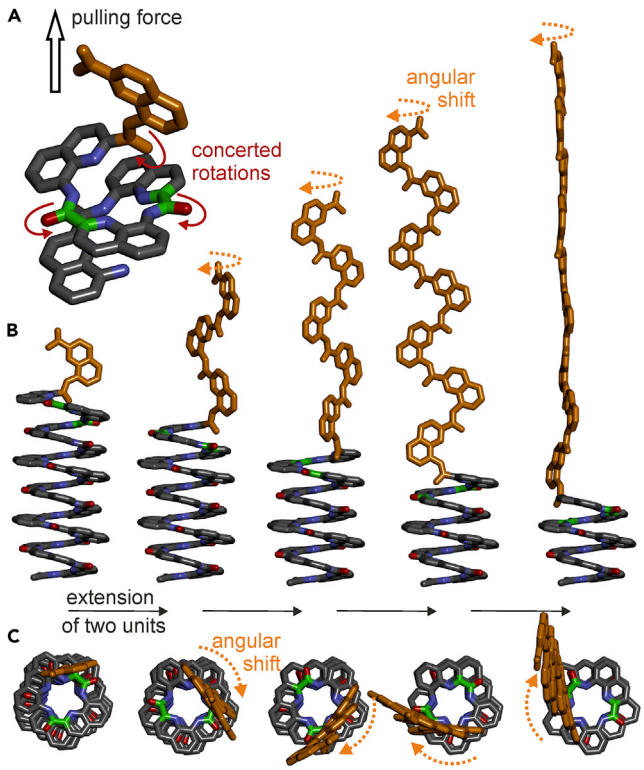

Figure 5. Unwinding model

(A) Fragment of a $\mathbf{Q}_n$ helix showing a plausible snapshot of the junction between helically folded (in gray tubes) and extended (in gold tubes) segments. Red arrows indicate the Cα-CO bonds about which concerted rotation would give rise to a two-unit extension. These bonds all belong to the upper first turn of the helix. The bonds shown in green are almost parallel and diametrically opposite; their concerted rotations would take place in opposite directions, in an accordion-like motion.

(B) Molecular models of a helix after each extension of two units.

(C) Top view of the models shown in (B). Because two units span almost one turn (exactly 0.8 turn), their unwinding induces minimal rotational strain. These models illustrate unwinding at the C terminus of the oligomer. Similar models can be built at the N terminus.

(see Supplemental information for details).[60–62] The purpose of a stochastic analysis is the following: the analysis of events in the window of observation can be used to infer past and future events only if the process is deterministic, periodic, or stationary. In the plateau regime, the values of force spectroscopy can only be viewed as stochastic events. A treatment to reach an understanding of this regime can only be made by a stochastic analysis. In the long time scale, stochastic phenomena are Brownian. At shorter times, they can present anomalous features/dynamics whose investigation provides information on the interaction of the main process with the environment where it takes place.

Figure 6 presents a summary of the results that were obtained by ensemble averaging over the time series (see also Figure S16). Pulling, i.e., unwinding, and relaxing, i.e., rewinding, were treated separately. The analysis starts from the evaluation of the second moment in time, that is, the mean square force (MSF). A Brownian process is identified by a linear growth in time of the MSF, that is a scaling exponent, γ, that is equal to 1. Any deviation from linearity describes processes that are called anomalous. Figure 6A shows that for the MSF there are two distinct time regimes both for unwinding and rewinding. At shorter times, of up to eight steps, i.e.,

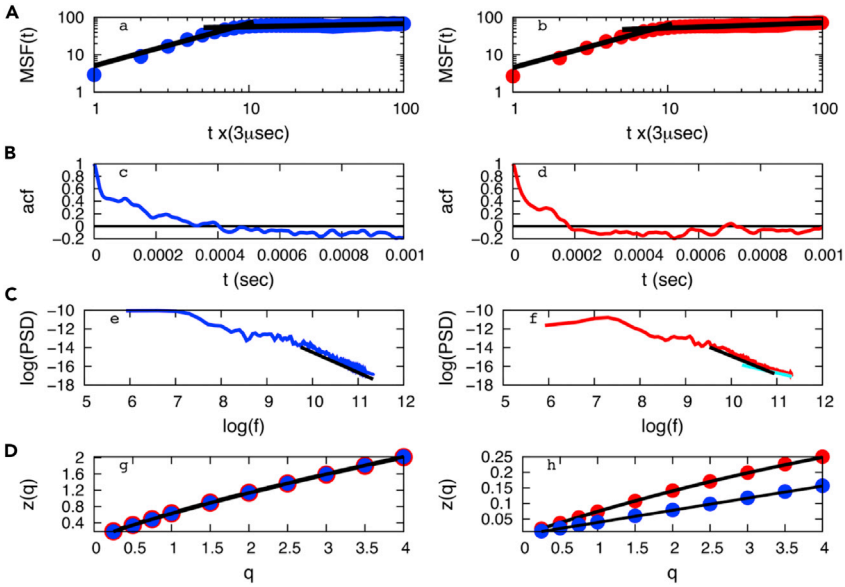

Figure 6. Anomalous diffusion object motion analysis

(A) Mean square force (MSF) versus time. The continuous black lines are the best fits to experimental data. Left: pulling, right: relaxing.

(B) Autocorrelation functions (acf). left: pulling, right: relaxing.

(C) Power spectral density (PSD) for all the experiments of Figure 3B. The short solid black lines are the slopes (red noise), and the short cyan line at the right describes flicker noise. Left: pulling, right: relaxing.

(D) Structure functions. Continuous black lines describe their analytical forms. Left: short times (<30 μs), right: long times (>30 μs). The parameters of fits of the structure functions had an error smaller than 0.9%. See also Tables S2–S4.

~24 μs, the force fluctuations are super linear with $\gamma = 1.14$. At longer times, the process changes very slowly, it is a strong sub-linear motion with scaling exponents $\gamma = 0.08/0.14$ for unwinding/winding. Figure 6B shows the autocorrelation function (ACF). In the short time regime identified for the MSF, the value of the ACF remains above 0.5 both for unwinding and winding. Both processes are persistent and correlated. In the short time regime, every subsequent step is more likely to keep the characteristics or direction of the previous one. If the system is winding, it will continue to wind; if it is unwinding it will persist in the unwinding. The time when the ACF goes to zero for the first time can be used to estimate the rate of the processes associated to the ACF, k. For unfolding, $k = 2{,}400\ s^{-1}$, for folding $k = 5{,}600\ s^{-1}$. These values are comparable to the fluctuation rate measured between wound and unwound states of about $7{,}500\ s^{-1}$ that was discussed above. Figure 6C shows the power spectral densities, PSD. At short times (smaller than 30 μs), or medium to high frequency, the slope approaches a value of 2 or a bit higher, which is the value of a red noise (Brownian or slight super-linear process), in agreement with the MSF. Interestingly, at even higher frequencies for the relaxing process, the slope takes a value of –1.1 (Figure 6C right panel, cyan solid line), which is associated to flicker noise, which, in turn, is a fingerprint of cooperativity. Figure 6D shows the structure functions, $z(q)$, where q is the order of the moment. The structure function (see Supplemental information for definitions) allows to determine the stochastic mechanism that govern the fluctuations.[60–62] At short times, the structure functions of pulling/relaxing are almost identical, $z(q) = Hq - Cq\ln(q)$ with $H = 0.627/0.633$ and $C = 0.088/0.094$ for pulling/relaxing. Unwinding and rewinding occur in a similar way. This form of the structure function is typical of a Cauchy-Lorentz probability for the distribution of the

fluctuations. The Cauchy distribution is often the distribution of observations for objects that are rotating or spinning, movements that are intrinsic to winding/unwinding. At longer times, pulling and relaxing take two very different forms of the structure function. For pulling, $z(q) = 0.039\ q$, the linear dependence of $z(q)$ describes a self-similar process that is monofractal and has a single or unique time scale. For relaxing, $z(q) = 0.074q - 0.004(q^2 - q)$. This form of the structure function is typical of a log normal probability for the distribution of the fluctuations. The lognormal distribution is often present in natural growth processes that take place by accumulation of small changes that are additive on a logarithmic scale. The structure function for the rewinding implies the presence of at least two random processes acting simultaneously. This makes the overall process multiplicative. These two random sequences of events likely could involve dynamics from both the helix and solvent molecules, which occur on two different timescales. Rewinding could be represented as the synchronization of the dynamics of all the molecules (helix and solvent) that click in together to squeeze out solvent molecules. This finding concurs with what is observed in proteins. The folding mechanism of these biosystems is governed by water molecules, which are crucially positioned in order to satisfy the Levinthal paradox.[63,64] A few water molecules bridge amino-acidic residues to form hydrogen bonds that drive the folding and avoid the sampling of the phase space which would take enormously long times to make the protein fold properly.

CONCLUSIONS

Muscle proteins constantly experience substantial mechanical load during muscle operation. α-helices have been identified as important components that reversibly unwind to mechanically protect proteins from dissociation.[46] Here, we have shown that the mechanics of synthetic helical aromatic oligoamides outperform that of these α-helices and of natural helices in general. Using AFM-based single-molecule force spectroscopy and statistical analysis, we were able to characterize both the elasticity and the free energy of the unwinding pathway of these synthetic helices. The analysis of the unfolding trajectories revealed that the molecules cooperatively unfold through the unwinding of two quinoline units in series, in agreement with their geometrical characteristics. They showed rapid fluctuations between wound and extended states, demonstrating the capacity of the molecules to develop high forces, up to 150 pN, when rewinding against the pulling force. The rewinding kinetics was shown to be extremely fast, which may be the consequence of a small number of rotatable bonds per helix turn. Pulling and relaxing cycles follow the same trace up to a very high loading rate of 5.10^4 pN s^{-1}. The free energy for unwinding was determined to be 150 kcal mol^{-1}, more than one order of magnitude greater than that of natural α-helices of similar length.

On top of the characterization of their single-molecule mechanics, these helices showed that they can sustain higher forces than natural α-helices and reversibly extend to 3.8 times their original length. The unprecedented and clear-cut elastic behavior of these systems suggest that practical applications may arise from their use as building blocks for the design of a new class of artificial elastomeric materials.

Furthermore, the deciphering of fast and defined folding trajectories enables some predictions. One may for example anticipate that aromatic helices having a larger diameter, that is, a lower curvature and more rotatable bonds per turn may unfold under lower forces, despite involving the same local non-covalent interactions. Investigations along these lines are in progress and will be reported in due course.

EXPERIMENTAL PROCEDURES

Resource availability

Lead contact

Further information and requests for data and reagents should be directed to and will be fulfilled by the Lead Contact, Anne-Sophie Duwez (asduwez@uliege.be).

Materials availability

The new compounds generated in this study require substantial time and resources for their preparation. Samples may be provided upon request pending their availability. Any request for advice to perform their synthesis following the protocols reported below is welcome.

Data and code availability

The force curves supporting the current study have not been deposited in a public repository for lack of a standard data presentation but are available from the lead contact on reasonable request.

SUPPLEMENTAL INFORMATION

Supplemental information can be found online at https://doi.org/10.1016/j.chempr.2021.02.030.

ACKNOWLEDGMENTS

F.D. thanks the Fonds de la Recherche Scientifique-Fonds National pour la Recherche Scientifique (FRS – FNRS) for her FRIA fellowship. The research was partly supported by the ERASMUS MUNDUS IDSFunMat program and by the European Research Council under the European Union's Seventh Framework Programme (ERC-2012- AdG-320892 to I.H.).

AUTHOR CONTRIBUTIONS

F.D. and X.L. performed the AFM experiments. F.D. and D.S. analyzed the AFM data. X.L. and V.M. carried out the compound synthesis and characterization studies. E.B. and F.Z. performed the ADOMA analysis. A.-S.D. and I.H. designed the experiments and directed the research. F.D., E.B., F.Z., I.H., and A.-S.D. prepared the manuscript. All the authors discussed the data and commented on the manuscript.

DECLARATION OF INTERESTS

The authors declare no competing interests.

Received: September 27, 2020
Revised: December 15, 2020
Accepted: February 26, 2021
Published: March 26, 2021

REFERENCES

1. Labeit, D., Watanabe, K., Witt, C., Fujita, H., Wu, Y., Lahmers, S., Funck, T., Labeit, S., and Granzier, H. (2003). Calcium-dependent molecular spring elements in the giant protein titin. Proc. Natl. Acad. Sci. USA *100*, 13716–13721.

2. Javadi, Y., Fernandez, J.M., and Perez-Jimenez, R. (2013). Protein folding under mechanical forces: a physiological view. Physiology *28*, 9–17.

3. Bao, G. (2009). Protein mechanics: a new frontier in biomechanics. Exp. Mech. *49*, 153–164.

4. Kuhlman, B., and Bradley, P. (2019). Advances in protein structure prediction and design. Nat. Rev. Mol. Cell Biol. *20*, 681–697.

5. Hoffmann, T., and Dougan, L. (2012). Single molecule force spectroscopy using polyproteins. Chem. Soc. Rev. *41*, 4781–4796.

6. Camunas-Soler, J., Ribezzi-Crivellari, M., and Ritort, F. (2016). Elastic properties of nucleic acids by single-molecule force spectroscopy. Annu. Rev. Biophys. *45*, 65–84.

7. Janshoff, A., Neitzert, M., Oberdörfer, Y., and Fuchs, H. (2000). Force spectroscopy of molecular systems-single moleculespectroscopy of polymers and biomolecules. Angew. Chem. Int. Ed. Engl. *39*, 3212–3237.

8. Fisher, T.E., Marszalek, P.E., and Fernandez, J.M. (2000). Stretching single molecules into novel conformations using the atomic force microscope. Nat. Struct. Biol. *7*, 719–724.

9. Bustamante, C., Chemla, Y.R., Forde, N.R., and Izhaky, D. (2004). Mechanical processes in biochemistry. Annu. Rev. Biochem. *73*, 705–748.

10. Neuman, K.C., and Nagy, A. (2008). Single-molecule force spectroscopy: optical tweezers, magnetic tweezers and atomic force microscopy. Nat. Methods *5*, 491–505.

11. Puchner, E.M., and Gaub, H.E. (2009). Force and function: probing proteins with AFM-based force spectroscopy. Curr. Opin. Struct. Biol. *19*, 605–614.

12. Liang, J., and Fernández, J.M. (2009). Mechanochemistry: one bond at a time. ACS Nano *3*, 1628–1645.

13. Duwez, A.-S., and Willet, N. (2012). Molecular Manipulation with Atomic Force Microscopy (CRC Press Press).

14. Hughes, M.L., and Dougan, L. (2016). The physics of pulling polyproteins: a review of single molecule force spectroscopy using the AFM to study protein unfolding. Rep. Prog. Phys. *79*, 076601.

15. Giannotti, M.I., and Vancso, G.J. (2007). Interrogation of single synthetic polymer chains and polysaccharides by AFM-based force spectroscopy. ChemPhysChem *8*, 2290–2307.

16. Oesterhelt, F., Rief, M., and Gaub, H.E. (1999). Single molecule force spectroscopy by AFM indicates helical structure of poly(ethylene-glycol) in water. New J. Phys. *1*, 6.

17. Marszalek, P.E., Oberhauser, A.F., Pang, Y.P., and Fernandez, J.M. (1998). Polysaccharide elasticity governed by chair-boat transitions of the glucopyranose ring. Nature *396*, 661–664.

18. Rief, M., Oesterhelt, F., Heymann, B., and Gaub, H.E. (1997). Single molecule force spectroscopy on polysaccharides by atomic force microscopy. Science *275*, 1295–1297.

19. Guichard, G., and Huc, I. (2011). Synthetic foldamers. Chem. Commun. *47*, 5933–5941.

20. Cheng, R.P., Gellman, S.H., and DeGrado, W.F. (2001). β-peptides: From structure to function. Chem. Rev. *101*, 3219–3232.

21. Yashima, E., Maeda, K., Iida, H., Furusho, Y., and Nagai, K. (2009). Helical polymers: synthesis, structures, and functions. Chem. Rev. *109*, 6102–6211.

22. Yashima, E., Ousaka, N., Taura, D., Shimomura, K., Ikai, T., and Maeda, K. (2016). Supramolecular helical systems: helical assemblies of small molecules, foldamers, and polymers with chiral amplification and their functions. Chem. Rev. *116*, 13752–13990.

23. Kim, J.S., Jung, Y.J., Park, J.W., Shaller, A.D., Wan, W., and Li, A.D.Q. (2009). Mechanically stretching folded nano- π-b; -stacks reveals pico-newton attractive forces. Adv. Mater. *21*, 786–789.

24. Sluysmans, D., Zhang, L., Li, X., Garci, A., Stoddart, J.F., and Duwez, A.S. (2020). Viologen tweezers to probe the force of individual donor−acceptor π-interactions. J. Am. Chem. Soc. *142*, 21153–21159.

25. Sluysmans, D., Willet, N., Thevenot, J., Lecommandoux, S., and Duwez, A.S. (2020). Single- molecule mechanical unfolding experiments reveal a critical length for the formation of α-helices in peptides. Nanoscale Horiz *5*, 671–678.

26. Lussis, P., Svaldo-Lanero, T., Bertocco, A., Fustin, C.A., Leigh, D.A., and Duwez, A.S. (2011). A single synthetic small molecule that generates force against a load. Nat. Nanotechnol. *6*, 553–557.

27. Van Quaethem, A., Lussis, P., Leigh, D.A., Duwez, A.-S., and Fustin, C.-A. (2014). Probing the mobility of catenane rings in single molecules. Chem. Sci. *5*, 1449–1452.

28. Sluysmans, D., Hubert, S., Bruns, C.J., Zhu, Z., Stoddart, J.F., and Duwez, A.S. (2018). Synthetic oligorotaxanes exert high forces when folding under mechanical load. Nat. Nanotechnol. *13*, 209–213.

29. Sluysmans, D., Devaux, F., Bruns, C.J., Stoddart, J.F., and Duwez, A.S. (2018). Dynamic force spectroscopy of synthetic oligorotaxane foldamers. Proc. Natl. Acad. Sci. USA *115*, 9362–9366.

30. Huc, I. (2004). Aromatic oligoamide foldamers. Eur. J. Org. Chem. *2004*, 17–29.

31. Zhang, D.W., Zhao, X., Hou, J.L., and Li, Z.T. (2012). Aromatic amide foldamers: structures, properties, and functions. Chem. Rev. *112*, 5271–5316.

32. Qi, T., Deschrijver, T., and Huc, I. (2013). Large-scale and chromatography-free synthesis of an octameric quinoline-based aromatic amide helical foldamer. Nat. Protoc. *8*, 693–708.

33. Jiang, H., Léger, J.M., and Huc, I. (2003). Aromatic δ-peptides. J. Am. Chem. Soc. *125*, 3448–3449.

34. Nelson, J.C., Saven, J.G., Moore, J.S., and Wolynes, P.G. (1997). Solvophobically driven folding of nonbiological oligomers. Science *277*, 1793–1796.

35. Gong, B., Zeng, H., Zhu, J., Yuan, L., Han, Y., Cheng, S., Furukawa, M., Parra, R.D., Kovalevsky, A.Y., Mills, J.L., et al. (2002). Creating nanocavities of tunable sizes: hollow helices. Proc. Natl. Acad. Sci. USA *99*, 11583–11588.

36. Ohkita, M., Lehn, J.M., Baum, G., and Fenske, D. (1999). Helicity coding: programmed molecular self-organization of achiral nonbiological strands into multiturn helical superstructures: synthesis and characterization of alternating pyridine-pyrimidine oligomers. Chem. Eur. J. *5*, 3471–3481.

37. Qi, T., Maurizot, V., Noguchi, H., Charoenraks, T., Kauffmann, B., Takafuji, M., Ihara, H., and Huc, I. (2012). Solvent dependence of helix stability in aromatic oligoamide foldamers. Chem. Commun. *48*, 6337.

38. Delsuc, N., Kawanami, T., Lefeuvre, J., Shundo, A., Ihara, H., Takafuji, M., and Huc, I. (2008). Kinetics of helix-handedness inversion: folding and unfolding in aromatic amide oligomers. ChemPhysChem *9*, 1882–1890.

39. Abramyan, A.M., Liu, Z., and Pophristic, V. (2016). Helix handedness inversion in arylamide foldamers: elucidation and free energy profile of a hopping mechanism. Chem. Commun. *52*, 669–672.

40. Li, X., Qi, T., Srinivas, K., Massip, S., Maurizot, V., and Huc, I. (2016). Synthesis and multibromination of nanosized helical aromatic amide foldamers via segment-doubling condensation. Org. Lett. *18*, 1044–1047.

41. Ziach, K., Chollet, C., Parissi, V., Prabhakaran, P., Marchivie, M., Corvaglia, V., Bose, P.P., Laxmi-Reddy, K., Godde, F., Schmitter, J.-M., et al. (2018). Single helically folded aromatic oligoamides that mimic the charge surface of double-stranded B-DNA. Nat. Chem. *10*, 511–518.

42. Chandramouli, N., Ferrand, Y., Lautrette, G., Kauffmann, B., MacKereth, C.D., Laguerre, M., Dubreuil, D., and Huc, I. (2015). Iterative design of a helically folded aromatic oligoamide sequence for the selective encapsulation of fructose. Nat. Chem. *7*, 334–341.

43. Méndez-Ardoy, A., Markandeya, N., Li, X., Tsai, Y.T., Pecastaings, G., Buffeteau, T., Maurizot, V., Muccioli, L., Castet, F., Huc, I., and Bassani, D.M. (2017). Multi-dimensional charge transport in supramolecular helical foldamer assemblies. Chem. Sci. *8*, 7251–7257.

44. Li, X., Markandeya, N., Jonusauskas, G., McClenaghan, N.D., Maurizot, V., Denisov, S.A., and Huc, I. (2016). Photoinduced electron transfer and hole migration in nanosized helical aromatic oligoamide foldamers. J. Am. Chem. Soc. *138*, 13568–13578.

45. Rief, M., Pascual, J., Saraste, M., and Gaub, H.E. (1999). Single molecule force spectroscopy of spectrin repeats: low unfolding forces in helix bundles. J. Mol. Biol. *286*, 553–561.

46. Berkemeier, F., Bertz, M., Xiao, S., Pinotsis, N., Wilmanns, M., Gräter, F., and Rief, M. (2011). Fast-folding alpha-helices as reversible strain absorbers in the muscle protein myomesin. Proc. Natl. Acad. Sci. USA *108*, 14139–14144.

47. Schwaiger, I., Sattler, C., Hostetter, D.R., and Rief, M. (2002). The myosin coiled-coil is a truly elastic protein structure. Nat. Mater. *1*, 232–235.

48. Li, L., Wetzel, S., Plückthun, A., and Fernandez, J.M. (2006). Stepwise unfolding of ankyrin repeats in a single protein revealed by atomic force microscopy. Biophys. J. *90*, L30–L32.

49. Takahashi, H., Rico, F., Chipot, C., and Scheuring, S. (2018). α-helix unwinding as force buffer in spectrins. ACS Nano *12*, 2719–2727.

50. Cluzel, P., Lebrun, A., Heller, C., Lavery, R., Viovy, J.L., Chatenay, D., and Caron, F. (1996). DNA: an extensible molecule. Science *271*, 792–794.

51. Smith, S.B., Cui, Y., and Bustamante, C. (1996). Overstretching B-DNA: the elastic response of individual double-stranded and single-stranded DNA molecules. Science *271*, 795–799.

52. Zhang, Q., and Marszalek, P.E. (2006). Identification of sugar isomers by single-molecule force spectroscopy. J. Am. Chem. Soc. *128*, 5596–5597.

53. Zhang, L., Wang, C., Cui, S., Wang, Z., and Zhang, X. (2003). Single-molecule force spectroscopy on curdlan: unwinding helical structures and random coils. Nano Lett *3*, 1119–1124.

54. Zegarra, F.C., Peralta, G.N., Coronado, A.M., and Gao, Y.Q. (2009). Free energies and forces in helix–coil transition of homopolypeptides under stretching. Phys. Chem. Chem. Phys. *11*, 4019–4024.

55. Zoldák, G., Stigler, J., Pelz, B., Li, H., and Rief, M. (2013). Ultrafast folding kinetics and cooperativity of villin headpiece in single-molecule force spectroscopy. Proc. Natl. Acad. Sci. USA *110*, 18156–18161.

56. Rico, F., Gonzalez, L., Casuso, I., Puig-Vidal, M., and Scheuring, S. (2013). High-speed force spectroscopy unfolds titin at the velocity of molecular dynamics simulations. Science *342*, 741–743.

57. Yu, H., Siewny, M.G.W., Edwards, D.T., Sanders, A.W., and Perkins, T.T. (2017). Hidden dynamics in the unfolding of individual bacteriorhodopsin proteins. Science *355*, 945–950.

58. Puchner, E.M., Franzen, G., Gautel, M., and Gaub, H.E. (2008). Comparing proteins by their unfolding pattern. Biophys. J. *95*, 426–434.

59. Uribe, L., Gauss, J., and Diezemann, G. (2016). Determining factors for the unfolding pathway of peptides, peptoids, and peptidic foldamers. J. Phys. Chem. B *120*, 10433–10441.

60. Parent, L.R., Bakalis, E., Ramírez-Hernández, A., Kammeyer, J.K., Park, C., de Pablo, J., Zerbetto, F., Patterson, J.P., and Gianneschi, N.C. (2017). Directly observing micelle fusion and growth in solution by liquid-cell transmission electron microscopy. J. Am. Chem. Soc. *139*, 17140–17151.

61. Parent, L.R., Bakalis, E., Proetto, M., Li, Y., Park, C., Zerbetto, F., and Gianneschi, N.C. (2018). Tackling the challenges of dynamic experiments using liquid-cell transmission electron microscopy. Acc. Chem. Res. *51*, 3–11.

62. Bakalis, E., Parent, L.R., Vratsanos, M., Park, C., Gianneschi, N.C., and Zerbetto, F. (2020). Complex nanoparticle diffusional motion in liquid-cell transmission electron microscopy. J. Phys. Chem. C *124*, 14881–14890.

63. Zwanzig, R., Szabo, A., and Bagchi, B. (1992). Levinthal's paradox. Proc. Natl. Acad. Sci. USA *89*, 20–22.

64. Karplus, M. (1997). The Levinthal paradox: yesterday and today. Fold. Des. *2*, S69–S75.